MAGNETIC EFFECTS
OF
THE QUIET TIME PROTON BELT

BY

R. A. HOFFMAN
AND
P. A. BRACKEN

JUNE 1964

MAGNETIC EFFECTS OF THE QUIET TIME PROTON BELT

by

R. A. Hoffman and P. A. Bracken

June 1964

Goddard Space Flight Center

Greenbelt, Maryland

ABSTRACT

2 9463

An analysis of the magnetic effects of the quiet time proton belt has been performed with data obtained from a proton detector aboard Explorer XII. From the measured energy spectra, intensities, and pitch angle distributions of the protons with energies above 100 kev, the current density on a magnetic meridian plane was calculated using the theory of Akasofu and Chapman, modified to eliminate several simplifying assumptions. The algebraic sum of all the currents was 0.59 million amperes, and the magnetic moment of the current loop was $0.029M_E$. From the electric current distribution the magnetic perturbations on the meridian plane were obtained. At the magnetic equator on the earth's surface the proton belt produced a 9 γ decrease in the field in comparison with the 38 γ decrease reported by Akasofu, Cain and Chapman based on some preliminary data from the same detector. The maximum perturbation appeared at L = 3.6 on the magnetic equator, where the field attained a value of -23 γ.

Author

I. Introduction.

The various motions which a group of charged particles exhibit when trapped in the earth's magnetic field result in electric currents. The analysis of these movements yields the observation that the net currents are parallel to lines of magnetic latitude: in some regions of space they flow eastward, and in other regions westward. If one assumes longitudinal symmetry about the earth, these motions necessarily correspond to a toroidal ring current encircling the earth.

On the basis of geomagnetic evidence it has long been postulated that some type of ring current exists. The enhancement of the current at times was thought to be one cause of magnetic activity, but even during magnetically quiet times the current was never supposed to die away completely.

Thus, since the advent of the satellite era and the discovery of the earth's trapped radiation, there has been considerable expectation that the particles which constitute the ring current would be directly observed, and their species, energies and spatial distributions determined. In addition, magneticians have sought the location of the currents by attempting to measure their magnetic effects with satellite borne magnetometers. While the trapped radiation was discovered over five years ago, the endeavor to observe any significant ring current has been unsuccessful until recently.

In an initial survey of data received from a low energy proton detector aboard Explorer XII (launched August 16, 1961), Davis and Williamson (1963) noticed that the energy density of the 100 kev to 4.5 Mev protons amounted

to an appreciable fraction of the energy density of the earth's magnetic

field during a magnetically quiet period, and from 4 out to 8 earth radii

the ratio of the two energy densities was almost constant. It was of obvious

interest to determine the magnitude of the magnetic field produced by this

population of protons. On the basis of some preliminary data furnished by

Davis, Akasofu, Cain and Chapman (1962) calculated the magnetic disturbance

for a model proton belt which resembled the measured proton distribution.

The results predicted a decrease in the surface equatorial field of about

38 γ due to the quiet time belt. Davis and Williamson (1963) also observed

a three fold increase in proton intensities at small pitch angles during a

magnetic storm. Adopting the assumptions that (1) this increase was

applicable to protons of all pitch angles, and (2) the average energy of

the particles equalled the quiet time energy, Akasofu and Cain (1962a)

calculated that an additional 80 γ decrease would be observed at the

equator of the earth, sufficient to account for the -60 γ main phase of the

aforementioned magnetic storm.

A considerably more thorough analysis of the magnetic effects of the

quiet time proton belt has now been performed from the data obtained from

the proton detector aboard Explorer XII, and the results are transmitted

in this paper. In addition to the fact that these protons produce the

greatest magnetic disturbance of any known population of trapped particles,

it is also of interest to study the effects of the ring current on

phenomena related to the earth's main magnetic field. The magnetic lines

of force are distorted from the shapes calculated by the spherical harmonic

analysis of the field at the earth's surface. There is a stretching out or strengthening of the field at distances beyond the ring current which affects the location of the magnetospheric boundary. Of interest to cosmic ray physicists is the influence of the Störmer cut-off rigidity for solar protons approaching the earth near the polar regions. Finally, the quiet time particle distributions are established in order to acquire a basis for determining storm time variations.

Thus, in this paper the proton data are also interpreted so as to determine the extent which the magnetic perturbations of the protons effect the earth's main field.

II. Proton Lifetimes.

The proton ring current under discussion has been described as a "quiet time" current, there being arguments against consideration that its enhancement during a magnetic storm is the cause of the main phase. If one assumes that the lifetimes of these particles are limited solely by coulomb scattering and charge exchange, the decay time of an enhanced current during a magnetic storm would be an order of magnitude larger than the one day recovery time indicated by magnetograms at ground level (Liemohn, 1961). To obtain agreement between the observed decay time and calculated proton lifetimes, it is necessary to postulate that protons in the energy region 1 to 100 kev (below the threshold of the Explorer XII detector) constitute the storm time ring current (Dessler, Hanson and Parker, 1961). In light of the fact that at magnetically quiet periods the observed proton intensities remain stable to within a factor of two over a long period of time (Davis, Hoffman and Williamson, 1964), the electric current resulting

from them is considered to exist at all times and is described as a quiet time ring current.

However, one must recognize the fact that an enhancement of the protons within the energy range of the detector might constitute the higher energy portion of the storm time particles. Since protons trapped at a given time do have finite lifetimes, there must be a source and probably an acceleration mechanism for replenishing the population. In view of the insufficiency of our knowledge concerning such processes, it is possible that the particular acceleration mechanism, and perhaps others, may influence the lifetimes of the particles. It has also been experimentally observed that during a magnetic storm some time variations do exist. For these reasons the storm time proton observations are being carefully analyzed and will be reported in a later paper.

III. Electric Currents.

Since the magnetic effects of the trapped protons are due to the electric currents they establish, it is first necessary to deduce the current distribution on a magnetic meridian plane from the experimental observations of the protons. For this calculation a slightly modified version of the theory developed by Akasofu and Chapman (1961) is used. Essentially the same notation has also been adopted and appears for reference in the Appendix.

In Alfven's guiding center approximation describing the motion of charged particles in a strong magnetic field, the motion is analyzed into three parts: (a) the gyration about and in a plane perpendicular to a magnetic field line; (b) the oscillation essentially along a line of

force between two mirror points; and (c) the east-west <u>drift</u> motion for positively charged particles on a magnetic shell. All of these motions may contribute to the flow of an electric current, i. To calculate the current produced in a gas permeated by a magnetic field, the gas pressure and the characteristics of the magnetic field must be known at every point in the gas.

We now limit the discussion to the steady state case with a proton distribution symmetrical about the axis of the magnetic poles. While the experimental data will be analyzed in the B/B_e (or equatorial pitch angle), L coordinate system, the computations will assume a geomagnetic dipole field. If $\hat{k}$ is the eastward unit vector normal to a magnetic meridian plane at a particular point, the volume current densities arising from the three motions are obtained from the following formulae (<u>Parker</u>, 1957):

a) The current produced by the gyration:

$$\vec{i}_L = \hat{k} \left[\frac{c}{aBh_2} \left(\frac{\partial P_n}{\partial L} - \frac{1}{2} \frac{P_n}{P_m} \frac{\partial P_m}{\partial L} \right) + \frac{c}{BR_c} P_n \right] \tag{1}$$

where

$$h_2 = \frac{\cos^3 \varphi}{(1 + 3\sin^2 \varphi)^{\frac{1}{2}}} = \frac{1}{\cos^3 \varphi} \left(\frac{B}{B_e} \right)^{-1} \tag{2}$$

and

$$\frac{1}{R_c} = \frac{3(1 + \sin^2 \varphi)}{aL \cos \varphi \ (1 + 3\sin^2 \varphi)^{3/2}} \ . \tag{3}$$

b) The current due to the oscillations:

$$i_o = enw_s = 0, \tag{4}$$

because as many particles are passing through a unit area perpendicular to B towards one mirror point as are moving towards the other mirror point, at least over a short period of time.

c) The current produced by the drift motion:

$$\vec{i}_D = \hat{k} \left(\frac{c}{2aBh_2} \frac{p_n}{p_m} \frac{\partial p_m}{\partial L} - \frac{c}{BR_c} p_s \right) \tag{5}$$

The total current is then

$$\vec{i} = -i\hat{k} \tag{6}$$

with

$$i = \frac{c}{BR_c} \left(p_s - p_n \right) - \frac{c}{aBh_2} \frac{\partial p_n}{\partial L} \tag{7}$$

The negative sign in equation 6 signifies that a positive term in i is a westward contribution to the current density, and a negative term is an eastward contribution.

Let us briefly consider just what details in the motions of the particles give rise to the three current terms of i. The first term involving p_s is due to the westward drift motion of protons which depends upon the centrifugal force mw_s^2/R_c associated with the motion along a curved field line.

The second term also arises from the curvature of the lines of force. The circular orbits due to the gyration are more crowded together on the concave side of the line than on the convex side. This is illustrated in Figure 1a, where between two adjacent lines of force there is a higher density of particles per unit area moving into the page than out of it.

For protons this results in a net eastward current at all points. Surprisingly, this term is larger than the term due to the drift motion if the pitch angle distributions are reasonably steep, as they are for the protons in the belt being discussed.

The final term is due to the fact that the radiation exists in a belt: the intensity increases with radial distance to a certain point, and then decreases. The effect in producing currents is illustrated in Figure 1b, in which the particle intensity is larger on the line of force at a greater distance from the earth, causing a more intense movement of charged particles in a direction into the page than out of it in the region between the lines of force where the two currents intersect. On the inner side of the belt the current will be eastward, and on the outer side it will be westward.

The calculation of the current at all points on a meridian plane first requires the determination of the pressures p_s and p_n at each point. To simplify the equations we first consider protons of a single speed w.

The longitudinal pressure $p_s{}^* = Nmw_s{}^2$.

The lateral pressure $p_n{}^* = \frac{1}{2}Nmw_n{}^2$.

While it would be possible to calculate these pressures at each point in the magnetosphere from the experimental data, considerable simplification is obtained if they can be expressed in terms of a few parameters determined by the particle distributions. This is accomplished by first fitting the data to a special equatorial pitch angle distribution function with which the local intensities and pitch angle distributions can be obtained from the equatorial intensity and distribution by means of a single parameter depending only upon L. Then the current equation is integrated over the energy spectrum

of the particles of interest at each L value; this integral turns out to be actually the total momentum flux at the equator. Hence, the local current at a given latitude depends only upon the two parameters representing the pitch angle distribution and equatorial momentum flux.

Let $F(L,s,\theta)$ denote the number density of protons at a point s on a magnetic shell L, whose speeds lie in dw at w, whose pitch angles lie in dθ at θ, and whose azimuth angle is arbitrary, since we assume symmetry in azimuth. Note that this definition of $F(L,s,\theta)$ is slightly different than that of Akasofu and Chapman (1961) in that it includes a differential angle in azimuth. Fortunately, we can also adopt Parker's special pitch angle distribution (Parker, 1957) for the functional form of the distribution in pitch angle, but with the conditions discussed in Section 4 "Proton Data" of this paper:

$$F(L,S,\theta) = C_\alpha \left(\frac{B_e}{B} \right)^{\frac{\alpha}{2}} \sin^\alpha \theta. \qquad (8)$$

This distribution has very useful and curious properties. It can be divided into two parts: the second part, $\sin^\alpha \theta$, is the local pitch angle distribution and has a form independent of B_e/B. Hence the ratio of p_n to p_s remains the same at every point on an L shell. Because the form function, $\sin^\alpha \theta$, is independent of B_e/B, the integral over all pitch angles, which would be evaluated to obtain the omnidirectional intensity at any value of B_e/B, is independent of this ratio of fields. Hence, the omnidirectional intensity varies down a line of force only as $(B_e/B)^{\frac{\alpha}{2}}$.

The constant C_α can be expressed in terms of the total density at the equator $N_e(L)$:

$$N_e(L) = C_\alpha \int_0^\pi \sin^\alpha \theta \ (2 \pi \sin \theta) \ d\theta \qquad (9)$$

The integral in $N_e(L)$ will arise again in the theory and can be expressed in terms of gamma functions:

$$\int_0^\pi \sin^{\alpha+1}\theta \ d\theta = \sqrt{\pi} \ \frac{\Gamma\left(\frac{\alpha+2}{2}\right)}{\Gamma\left(\frac{\alpha+3}{2}\right)} \qquad (10)$$

Hence

$$C_\alpha = \frac{1}{2} \pi^{-3/2} \ \frac{\Gamma\left(\frac{\alpha+3}{2}\right)}{\Gamma\left(\frac{\alpha+2}{2}\right)} \qquad N_e(L) = A(\alpha)N_e(L) \qquad (11)$$

Therefore

$$F(L,s,\theta) = N_e(L) \ A(\alpha) \left(\frac{B_e}{B}\right)^{\frac{\alpha}{2}} \sin^\alpha \theta. \qquad (12)$$

Since a particle detector measures a flux rather than a density it would be well to express all equations in terms of fluxes.

$$F(L,s,\theta) = \frac{I_e(L)}{w} \ A(\alpha) \left(\frac{B_e}{B}\right)^{\frac{\alpha}{2}} \sin^\alpha \theta \qquad (13)$$

where $I_e(L)$ is the omnidirectional intensity at the magnetic equator as a function of L for protons of speed w. It must be noted that α is a function of L, and could also depend upon w.

Inserting this expression into the formulae for the gas pressures

yields for protons with speed w:

$$p_s{}^* = m \int_0^\pi (w^2\cos^2\theta) \; \frac{I_e(L)}{w} \; A(\alpha) \left(\frac{B_e}{B}\right)^{\frac{\alpha}{2}} \sin^\alpha \theta (2 \pi \sin \theta) \, d\theta \qquad (14)$$

and

$$p_n{}^* = \frac{m}{2} \int_0^\pi (w^2\sin^2\theta) \; \frac{I_e(L)}{w} \; A(\alpha) \left(\frac{B_e}{B}\right)^{\frac{\alpha}{2}} \sin^\alpha \theta \; (2 \pi \sin \theta) \, d\theta \qquad (15)$$

Evaluating the integrals with the aid of equation 10, we have

$$P_n{}^* = \frac{1}{2} \, mwI_e(L) \, \Omega \, (\alpha)\left(\frac{B_e}{B}\right)^{\frac{\alpha}{2}} \qquad (16)$$

where

$$\Omega \, (\alpha) = \frac{\alpha+2}{\alpha+3} \qquad (17)$$

and

$$p_s{}^* = \frac{2}{\alpha+2} \; p_n{}^*, \qquad (18)$$

which indicates again that the ratio of partial pressures is constant on an L shell.

The current can now be expressed in terms of $I_e(L)$ and α:

$$i^* = \frac{c}{BR_c} \frac{\alpha}{\alpha+2} P_n^* - \frac{c}{aBh_2} \frac{\partial P_n^*}{\partial L}$$

$$= -\frac{c}{BR_c} \frac{\alpha}{\alpha+3} \frac{1}{2} mw I_e(L) \left(\frac{B_e}{B}\right)^{\frac{\alpha}{2}}$$

$$-\frac{c}{aBh_2} \frac{1}{2} mw \left[\Omega(\alpha) \left(\frac{B_e}{B}\right)^{\frac{\alpha}{2}} \frac{\partial I_e(L)}{\partial L} + \left(\frac{B_e}{B}\right)^{\frac{\alpha}{2}} I_e(L) \right.$$

$$\left. + \frac{1}{2} I(L) \Omega(\alpha) \left(\frac{B_e}{B}\right)^{\frac{\alpha}{2}} \ln\left(\frac{B_e}{B}\right) \frac{\partial \alpha}{\partial L} \right] \quad (19)$$

or

$$i^* = -\frac{mwc}{aH_o} \left[D^*(\alpha,\varphi)L^2 I_e(L) + E^*(\alpha,\varphi)L^3 \frac{\partial I_e(L)}{\partial L} + F^*(\alpha,\varphi)L^3 I_e(L) \frac{\partial \alpha(L)}{\partial L} \right] \quad (20)$$

where H_o is the field strength on the equator at the earth's surface, and

$$D^*(\alpha,\varphi) = \frac{3}{2} \left(\frac{B_e}{B}\right)^{\frac{\alpha}{2}+4} \frac{\alpha}{\alpha+3} \frac{(1+\sin^2\varphi)}{\cos^{19}\varphi} ,$$

$$E^*(\alpha,\varphi) = \frac{1}{2} \frac{\alpha+2}{\alpha+3} \left(\frac{B_e}{B}\right)^{\frac{\alpha}{2}} \cos^3\varphi , \quad (21)$$

$$F^*(\alpha,\varphi) = E^*(\alpha,\varphi) \left[\frac{1}{(\alpha+2)(\alpha+3)} - \frac{1}{2} \ln\left(\frac{B}{B_e}\right) \right]$$

Equation 20 corresponds to equation 52 of <u>Akasofu</u> <u>and</u> <u>Chapman</u> (1961) with the added term depending upon α (L).

It is now necessary to integrate the current over the energy range measured by the detector. Since the scintillator has a low energy cut-off near 100 kev, the current density distribution arising from protons with energies greater than 100 kev will be calculated. This low energy limit must be kept clearly in mind in what follows.

We next make another simplifying assumption: that α is independent of energy, or the energy spectrum is a function only of L, not of pitch angle. The validity of this assumption will be discussed in Section 4, "Proton Data." This allows D*, E*, and F* to be independent of energy.

The only terms remaining in the current equation 20 which depend upon energy are the velocity w and the equatorial omnidirectional flux of this velocity, I(L), which is actually the omnidirectional differential energy spectrum, $\frac{dN}{dE}$. Let

$$\psi(L) = \int_{100}^{\infty} mw \frac{dN}{dE} dE = 2m \int_{100}^{\infty} \sqrt{E} \frac{dN}{dE} dE,$$

which is a momentum flux, or twice the energy density of the protons. Then

$$i = -\frac{c}{aH_o} \left[D(\alpha,\varphi) L^2 \psi(L) + E(\alpha,\varphi)L^3 \frac{d\psi(L)}{dL} + F(\alpha,\varphi)L^3 \psi(L) \frac{d\alpha(L)}{dL} \right] \qquad (23)$$

Hence, the current at any point in space, L, φ, need be expressed only in terms of the pitch angle parameter α and the momentum profile ψ at the equator.

IV. Proton Data.

The data relating to the low energy protons from which the current distributions have been calculated were acquired from one orbit of the satellite, pass 10A (outbound) and 10B (inbound) on August 27 and 28, 1961. At this time the major axis of the orbit was lying in the meridian plane which included the sun (see Figure 2). Since the heart of the proton belt (L = 3.5) lies at a relatively low altitude in comparison with apogee (L = 13) much of the data were collected near the twilight regions, although the outer edge of the belt was traversed on the sunlit side of the earth.

The planetary magnetic three-hour-range index K_p, plotted in Figure 3, indicated that no major disturbances were in progress. In fact the first appreciable magnetic disturbance during the lifetime of Explorer XII did not occur until pass 12.

This particular pass was chosen for thorough analysis because the orbit lay closer to the geomagnetic equator in the heart of the belt than any other orbit. Also the telemetry coverage was complete. When this study was initiated it was expected that a very typical proton distribution would be observed during the pass 10, since Davis and Williamson (1963) found no temporal variations larger than 30% during nineteen passes of Explorer VII distributed before and after this pass, but not including it. However, later comparisons with this original data indicate that the

proton intensities were enhanced by as much as a factor of two at L values smaller than the maximum intensity at L of 3.5 during pass 10. The maximum was also somewhat sharper than observed on the average pass with a more rapid decrease in intensity with increasing L beyond the maximum. This means that the belt was lying at slightly smaller L values than the average belt.

The details of the low energy proton detector have been described by Davis and Williamson (1963). Let it suffice here to produce a table containing the spectra employed in calculating the momentum integral ϕ (Table 1), as well as some examples of pitch angle distributions. In general the energy spectrum was described as a doubly sloped exponential spectrum, illustrated in Figure 4 in the integral form which was actually measured by the detector. At L values below 2.2 the data points were best fit with power law spectra, and up to L of 3 a steep power law spectrum was included for the higher energy protons, as suggested by the data of Bame et al (1963) and Naugle and Kniffen (1963). The spectra listed in Table 1 were differential before insertion into the momentum integral.

In the derivation of the formulae from which the current distributions may be computed, considerable simplification was attained by employing as the functional form of the pitch angle distribution, $\sin^\alpha \theta$. The measured angular distributions were found to fit this form reasonably well provided the entire range of pitch angles, 90° to 0°, was divided into two regions, 90° to 30°, and 30° to 0°, each with an independently determined value of α. Some sample fits of the data to this function appear in Figure 5.

Figure 5a illustrates the extrapolation to 90° of the distribution based on data points with pitch angles only between 30° and 56°. At low L values the orbit carried the satellite away from the magnetic equator making the measurement of protons with large pitch angles impossible. Figure 5b is an excellent example of the necessity of using the two independent values of α. An attempt at a least squares fit of all data from 0° to 90° produced a curve (solid line) with a large hump at the middle pitch angles and a very low value at large pitch angles.

Another assumption which considerably simplified the derivation of the current distribution formulae involved the independence of α upon energy. In reality the value of α increases as a function of increasing energy, as illustrated by the data in Figure 6 for protons of equatorial pitch angles between 90° and 30°. The data in the figure were obtained from the output of the detector which measured the incident energy flux of protons rather than the particle flux. The energies at which the points are plotted are the effective low energy cut-offs for the integral energy spectrum measured at this value of L. By choosing a constant value of α for a given L, the functions D^*, E^*, and F^* (equation 21) became energy independent and could be removed from the integration over energy. Hence, the value of α (L) selected is approximately the value derived for the particles having the average momentum on the given L shell. This value of α as a function of L is plotted in Figure 7 for each of the two pitch angle ranges, 90° to 30°, and 30° to 0°.

The calculation of N_{0I}, employed in the determination of the momentum integral ψ (see Figure 4 for spectral shape of the ψ integral), required some special attention. This quantity, the integral omnidirectional

intensity above zero energy, is equivalent to the directional intensities

at 100 kev integrated over all pitch angles, which can be actually measured

by the detector, multiplied by the factor $\exp(100/E_o)$. However, the

counting rates of the lowest energy channels of the detector aboard

Explorer XII passed into saturation about one earth radius on either

side of the maximum intensity at 3.5 R_E, at least at large pitch angles.

Hence, it was necessary to compute N_{OI} by either of two less direct methods.

If (1) a directional intensity above an energy E_c, $J(> E_c)$, is measured

at a pitch angle θ_c, (2) the pitch angle distribution characterized by the

parameter α is known, and (3) the energy spectrum (E_o) is measured (the

latter two parameters could be determined by the current channels of the

detector, which did not pass into saturation), then the value of N_{OI} can

be calculated from the formulae

$$N_I(> E) = \frac{J(> E_c)}{G_o \sin^\alpha \theta_c} \; 2\pi^{3/2} \frac{\Gamma\left(\frac{\alpha+2}{2}\right)}{\Gamma\left(\frac{\alpha+3}{2}\right)} \exp\left[(E_c-E)/E_o\right] , \qquad (24)$$

where G_o is the telescope factor $= 5.85\times10^{-3}$ cm^2-ster., the expression

$2\pi^{3/2}$ times the gamma functions arises from integration over the pitch

angles, $(\sin^\alpha \theta_c)^{-1}$ is actually an extrapolation of the directional intensity

measured at θ_c to the intensity at 90° equatorial pitch angle, and

$\exp\left[(E_c-E)/E_o\right]$ is an extrapolation in energy from the integral point

at E_c to the energy E. The quantity N_I is then the integral omnidirection

flux above the energy E, so N_{OI} would have E = 0.

Therefore, when the counting rate channel at 100 kev was in saturation either of two extrapolations could be used to acquire N_{OI}: A higher energy channel (for example, the 880 kev step) would provide a non-saturated counting rate at a near 90° pitch angle, making $(\sin^{\alpha} \theta_c)^{-1} \cong 1$ but requiring an extrapolation in energy $\exp\left[(E_c-E)/E_0\right]$, or a smaller pitch angle measurement from the 100 kev channel would provide a measurement of $J(> E_c)$ out of saturation, allowing $\exp\left[(E_c-E)/E_0\right]$ to be near one, but increasing the value of $(\sin^{\alpha} \theta_c)^{-1}$. Obviously the accuracy of either method depends upon how well the data can be characterized by the parameters α and E_0. The values of N_{OI} employed in the computation of ψ (L) were acquired by utilizing both methods. Table II shows a sample set of intensities calculated for an L value of 3.25 for particles with pitch angles 30° to 90°. The agreement between the various calculations of an N_{OI} at a given L value was within $\pm 15\%$.

From the two sets of values of α (L) necessary to describe the protons over the entire pitch angle range from 0° to 90°, a double set of N_{OI} is calculated, since this quantity is a function of α through equation 24. Hence, we obtain two independent profiles of ψ (L), one to be associated with protons having pitch angles 30° to 90°, the other with protons from 0° to 30°. These two profiles appear in Figure 8.

V. Electric Current Distribution

The data have now been compiled in a form sufficient for the calculation of the electric current distribution from equation 23. One must keep in mind that the current at a particular L, φ is actually a function of the local partial pressures p_s and p_n (equation 7), but

we have replaced the problem of calculating them by utilizing the parameters α (L) and ψ (L). The set of these parameters which is applicable to the radiation at the point of calculation of i must be used. Since a proton with an equatorial pitch angle of 30° mirrors at a magnetic latitude of 32°, the calculation of i for latitudes less than 32° will employ the set of parameters describing protons with equatorial pitch angles from 30° to 90°, and the calculation of i for latitudes greater than 32° will utilize the parameters for protons of pitch angles 0° to 30°. There will be a discontinuity in i as a function of latitude at 32° because as this latitude is approached from the equatorial side, the parameters less accurately describe the actual radiation.

Two other discontinuities which arise in the distribution of i over a meridian plane are due to the approximation of α (L) and ψ (L) by the simple mathematical expressions listed in Table III. Except for ψ (L) in the region L = 2.25 to 2.75 for protons with 30° to 90° pitch angles, and L = 2.75 to 3.25 for 0° to 30° pitch angles, both α and ψ could be well approximated by either straight lines or exponentials. While the approximation curves are continuous, their derivatives contain discontinuities between the segments of the curves. Hence, since i depends upon the derivatives, it will contain discontinuities.

The calculations of i in both pitch angles ranges have been performed for the region of L from 1.5 to 10 in intervals of 0.1 and latitude from the equator down an L shell to approximately 1000 km above the surface of the earth in 2° intervals by utilizing an IBM 7094 computer at Goddard Space Flight Center. Actually the calculations were terminated at a latitude

within 2° of the latitude where the line of force attained a height of 1000 km. This convention was adopted so that a constant latitude increment could be used in the numerical integration involved in the magnetic field calculations. A contour plot of the current distribution on a magnetic meridian plane appears in Figure 9.

The contributions of each of the terms in equation 23 to the total current are displayed in Figure 10 for two different L shells, one on the inner side of the belt where the total current is eastward, the other on the outer side of the belt where the total current is westward. One notices from an inspection of Figures 9 and 10 that the westward portion of the ring current, producing a southward perturbing magnetic field on the earth's surface, arises from the second term J_2, which depends upon the gradiant of the momentum flux on the outer side of the belt.

Since the discontinuities in i appearing in these figures originate in the mathematical expressions used to fit the parameters appearing in the equation for i, a smoothed version of the current contour plot to illustrate the dominant features of the current distribution appears in Figure 11.

An integration has been performed to obtain the total eastward and westward currents, their algebraic sum, and the magnetic moment of the ring current. These values are tabulated in Table IV.

VI. Magnetic Field Of The Ring Current.

The magnetic field due to the ring current may be denoted by its components H_p and H_z respectively perpendicular and parallel to the dipole axis. These components refer to a point (r, φ) specified by its polar coordinates (φ is latitude) or alternatively by a point (af, φ) in L space

where $f = L \cos^2\varphi$.

The ring current region is then divided into elements dS_3 specified by (r', φ') in polar coordinates or by (af', φ') in L space, where $f' = L'\cos^2\varphi'$. Then (Stratton, 1941),

$$H_p = - \frac{2}{(acf \cdot \cos\varphi)} \int\!\!\int (f \sin\varphi - f'\sin\varphi') \left[E(k^2) - K(k^2) \right.$$

$$\left. + (2f \cdot f'\cos\varphi \cdot \cos\varphi') \frac{E(k^2)}{F_-^2} \right] (1/F) \, dS_3 \tag{25}$$

and

$$H_z = - \frac{2}{(ac)} \int\!\!\int \left[K(k^2) - E(k^2) + 2f'\cos\varphi'(f'\cos\varphi' - f \cos\varphi) \frac{E(k^2)}{F_-^2} \right] (1/F) dS_3 \tag{26}$$

Here $K(k^2)$ and $E(k^2)$ denote the complete elliptic integrals of the first and second kind respectively, and

$$k^2 = \frac{(4f \cdot f'\cos\varphi'\cos\varphi)}{F^2} \, ,$$

$$F_-^2 = f^2 + f'^2 - 2f \cdot f'\cos(\varphi - \varphi') \, ,$$

$$F^2 = f^2 + f'^2 + 2f \cdot f'\cos(\varphi + \varphi') \, .$$

An element of cross sectional area of the ring current region in the meridian, dS_3, is expressed as $dS_3 = a^2 L'\cos^4\varphi' dL' d\varphi'$.

The foregoing formulae appear as in Akasofu and Chapman (1961) except for the correction of several misprints.

The components H_p and H_z were calculated separately at each point in the specified current region for particles in both pitch angle intervals.

The results were then combined to give the total field components at each point in the current region for all ring current particles.

The integrations involved in calculating these field components were performed numerically on the IBM 7094 computer at Goddard, and the results appear in Figure 12. As with the current calculation, increments of 0.1 in L and 2° (0.0349 radian) in latitude were used.

A discontinuity in the components H_p and H_z arises when $L = L'$ and $\varphi = \varphi'$, since in this case $F_-^2 = 0$, which appears in the denominator of the argument for each field component. The contribution to the components from the element of integration causing this discontinuity was taken to be zero each time such a discontinuity appeared.

The coordinate system used indicates a negative H_z is in a southerly direction and a negative H_p points toward the earth.

VII. Discussion.

    (a) Vector Field of the Ring Current.

At the magnetic equator on the surface of the earth the magnetic field due to the ring current attained a value of 9 γ in a southern direction, a value considerably smaller than the 38 γ obtained by Akasofu, Cain and Chapman (1962) from the preliminary data from the same detector. A reasonable error analysis on the field strength appears virtually impossible to perform. Purely an estimate would place a confidence of about 50% ($\pm 5 \gamma$) on the field calculations.

The distribution of field vectors from the ring current which appears in Figure 12 indicates a field fairly uniform on the inside of the proton belt and parallel to the dipole axis, as expected. In the region of the belt the field shows considerable curl and achieves a maximum value of

23 γ on the equator at an L of 3.6. Outside the belt the field becomes parallel to the earth's field, but has the extremely small value of 2.5 γ. Hence, the ring current field due to these protons above an energy of 100 kev would have little influence on the shape of the boundary of the magnetosphere.

(b) Second Order Calculation.

While these protons with energies above 100 kev are showing some magnetic influence, the magnitude is not sufficient to perturb appreciably the magnetic field of the magnetosphere which arises from sources internal to the earth. In fact it appears that the distortion of the field even at the altitudes of the ring current due to the compression of the field by the solar wind is comparable to the disturbance from the ring current (Cahill and Amazeen, 1963). Hence the assumption of analyzing the data in the L, equatorial pitch angle coordinate system for the ring current calculations will produce results as accurate and physically meaningful as would an attempt at a second order calculation (Beard, 1962; Akasofu, Cain and Chapman, 1961), in which the trapped protons are assumed to move in a magnetic field differing from the internal field by the field of the ring current itself.

(c) Cut-off Rigidity of Solar Protons.

In order to explain the observations of low-rigidity solar protons near the earth at latitudes well below those predicted by normal Störmer theory, investigators have included the magnetic effects of a ring current as well as the termination of the geomagnetic field (Kellogg and Winckler, 1961; Akasofu, Lin and Van Allen, 1963; Ray, 1964). In order that a ring current contribute significantly to a reduction in the cut-off rigidity,

its magnetic moment must be some appreciable fraction of the magnetic moment of the earth. However, the moment due to the quiet time protons with energies above 100 kev is calculated to be only 0.029 that of the earth, a value much too small to affect solar proton trajectories.

(d) Model Belt Parameters.

On the basis of some very preliminary data from the proton detector aboard Explorer XII, the magnetic affects of a model belt that resembled the measured belt were calculated (Akasofu, Cain and Chapman, 1962). Since then the properties of a similar belt have been applied to various problems of a geophysical nature (see especially the later articles by Akasofu; Vestine, 1963). For this work the following parameters have been utilized to characterize the distribution of protons:

r_o: distance where the number density attains its maximum value,

g_1: Gaussian parameter for the inner side of the belt:
$n = n_o \exp(-g_1^2 z^2)$, where $z = (r - r_o)/a$,

g_2: Gaussian parameter for the outer side of the belt,

α: pitch angle parameter,

n_o: maximum number density,

E: average energy of all protons in the belt.

In table V are listed the values adopted in the literature and a set of suggested values which more accurately produce the results obtained in this more thorough study.

(e) Lower Energy Protons.

One must keep clearly in mind in this discussion of the magnetic properties of the trapped protons that only those with energies above 100 kev, the low energy cutoff for the direct detection of proton

particle fluxes by the detector, have been considered. However, in another mode of operation the detector could measure proton energy fluxes down to energies of some tens of kev, depending upon the steepness of the spectrum. Beginning at about an L of 5, large fluxes of protons were apparently present with energies extending down to at least 50 kev, and the ratio of the flux between 50 and 100 kev to that above 100 kev became increasingly large with range.

While a complete saturation of the field beyond five earth radii with very low energy protons would significantly contribute to a quiet time ring current, the maximum field produced at the earth's surface by such a particle distribution is insufficient to account for large magnetic storms.

For a rough estimation of this maximum field first assume that the particle energy density is limited by the energy density of the field on the magnetic equator of an L shell. Next assume that the particle intensity is isotropic ($\alpha = 0$) and hence constant everywhere on an L shell to latitudes of 60°, which is essentially the surface of the earth for $L \geq 5$. Using equation 23 with $1/h_2$ add $1/R_c$ evaluated at the equator, their maximum values, and with

$$\psi (L) = 2 \frac{H_o^2}{8 \pi L^6}$$

the current is

$$i(L) = \frac{cH_o}{2 \pi a L^4} \cos^3 \varphi$$

This produces a field at the center of the earth, and approximately at the surface, of

$$H_z = - \frac{1 \times 10^4}{\mathcal{L}^3} \gamma,$$

where $\mathcal{L}$ is the minimum distance of the belt from the center of the earth. For $\mathcal{L} = 5$, H_z is -76 γ, which is one, and probably two, factors of two too large if compared with a field derived from any realistic distribution of particles exactly calculated.

To account for a large storm of 300 γ (excluding inductive effects in the earth) the field would have to be saturated down to at least an L of 3.2, and probably more like 2.5 for a more reasonable particle distribution. The apparent necessity for such a high intensity, low altitude belt leads one to question whether the current equation 7 includes all the necessary terms to account for the ring current as it naturally occurs. One is tempted to suggest that electric fields may assist in the production of an increased westward movement of the protons already observed. It certainly would seem reasonable to attempt a measurement of electric fields in this region of space.

It is interesting to note that the lifetime of 50 kev protons at 5 earth radii is only on the order of a week (Liemohn, 1961). In order to sustain a quiet time belt of such particles it would be necessary to have a source which operates continually.

In passing it is perhaps well to mention that the trapped electrons observed to date produce negligible magnetic fields. Since the magnetic properties of a particle depend upon the square root of its mass, electron

fluxes of the order of 10^{10} electrons/cm^2-sec would be required to produce magnetic effects equivalent to those of the protons observed. This flux is two orders of magnitude greater than any reported in the literature.

VIII. Conclusions.

The protons with energies above 100 kev observed by the low energy proton detector flown by Davis and Williamson aboard Explorer XII are the first group of particles discovered in the trapped radiation region with intensities sufficient to produce significant magnetic effects. However, for applications to other geophysical problems, such as the distortion of field lines, the change in the Störmer cut-off rigidities, and the quiet time remains of a storm time ring current, the observed particle intensities are probably disappointingly small.

For future studies of the proton ring current two improvements in the data acquisition would be desirable. The orbit of the satellite should be more nearly equatorial over all L values, and the detectors should be capable of measuring protons down to nearly one kev in energy.

While this detector has provided information which has advanced our knowledge of the ring current problem, it appears that the complete understanding of the phenomenon will require some years of continued research with new particle detectors and possible complementary measurements of electric fields or a more complete understanding of other source mechaniams for the electric currents.

ACKNOWLEDGEMENTS

APPENDIX

Notation

a = earth's radius, in cm.

c = speed of light, in cm/sec.

r = radial distance from the center of the earth to a point of interest, in cm.

L = McIlwain's coordinate, in earth radii.

B = magnetic field vector, in gauss.

P_m = magnetic pressure = $B^2/8\pi$.

m = mass of a trapped particle in grams.

e = magnitude of charge of a trapped particle, in esu.

w = velocity of a particle, in cm/sec.

w_s = component of w along B.

w_n = component of w normal to B.

E = kinetic energy of a particle, in kev.

N = number density of particles.

θ = pitch angle of a trapped particle, i.e. the angle between w and B, or its complement if larger than $90°$.

P_s = pressure of the gas (trapped particles) along B.

P_n = pressure of the gas normal to B.

φ = geomagnetic latitude.

Note: the subscript "e" indicates that a quantity is being evaluated at the magnetic equator.

TABLE I

PROTON ENERGY SPECTRA

L	30° - 90° Equatorial Pitch Angles				0° - 30° Equatorial Pitch Angles			
	N_{OI}	E_o	E'	E_1	N_{OI}	E_o	E'	E_1
1.8	POWER LAW				POWER LAW			
2.0	SPECTRA				SPECTRA			
2.2				662[1]	4.69×10^7	625	1650	--[3&4]
2.5	2.04×10^8	635	1000	--[2]	1.46×10^8	515	1650	--[3]
2.8	2.17×10^8	456	1000	--[2]	3.07×10^8	390	900	725[5]
3.0	4.20×10^8	303	900	550[3]	4.15×10^8	255	900	320[3]
3.25	5.07×10^8	222	1000	480	4.22×10^8	205	900	480
3.5	6.10×10^8	193	880	300	4.64×10^8	185	900	226
3.7	4.88×10^8	196	880	196	3.40×10^8	176	∞	--
3.9	3.60×10^8	195	880	247	2.50×10^8	145	900	260
4.6	3.00×10^8	110	255	187	1.68×10^8	105	∞	--
5.0	2.80×10^8	73	255	139	1.73×10^8	61.5	255	90
5.5	1.62×10^8	68	350	148	1.14×10^8	52	∞	--
6.0	2.05×10^8	50	375	275	2.20×10^8	36	∞	--
7.05	1.35×10^8	33.5	--	∞	6.13×10^7	33	∞	--

Notes: All energies in kev.

(1) E_1 = 662 kev from 470 to 1000 kev; for E > 1000 kev, power law with γ for integral spectrum = 4.2. From 140 to 470 kev, no protons.
(2)   For E > 1000 kev, power law with γ = 4.2.
(3)   For E > 1650 kev, power law with γ = 4.2.
(4)   Below E = 255 kev, no protons.
(5)   For E > 2000 kev, power law with γ = 4.2.

TABLE II

E_c (kev)	θ_c	α	E_o (kev)	N_{OI}
105	40°	2.5	222	5.01×10^8
470	30°	2.5	222	5.34×10^8
880	70°	2.5	222	4.87×10^8

TABLE III
30° to 90° E.P.A.

α	L Region	ψ	L Region
$-1.07L + 6.36$	1.5 to 3.7	$2.95 \times 10^{-11} \exp(L/0.256)$	1.5 to 2.4
$-0.12L + 2.84$	3.7 to 10.0	$1.98 \times 10^{-7} \exp(L/4.12)$	2.7 to 3.5
		$3.50 \times 10^{-5} \exp(-L/0.810)$	3.5 to 10.0

0° to 30° E.P.A.

α	L Region	ψ	L Region
$-1.62L + 6.57$	1.5 to 2.5	$2.06 \times 10^{-12} \exp(5.18L)$	1.5 to 2.0
$0.52L + 1.22$	2.5 to 3.0	$4.23 \times 10^{-10} \exp(2.52L)$	2.0 to 2.75
$27.5L^{-2.113}$	3.0 to 5.3	$5.91 \times 10^{-5} \exp(-1.476L)$	3.2 to 10.0
$-0.053L + 1.16$	5.3 to 10.0		

In the regions of ψ not included by these formulae, tabulated values from the curves of Figure 8 were used.

TABLE IV

	esu/sec	amps
Eastward Current	0.57×10^{15}	0.19×10^{6}
Westward Current	2.34×10^{15}	0.78×10^{6}
Total Current	1.77×10^{15}	0.59×10^{6}

Magnetic Moment $0.029 M_E$ ($M_E = 8.1 \times 10^{25}$ gauss-cm^3)

TABLE V

Parameter	Value in Current Literature	Revised Value
r_0	3.0 and 3.2	3.5
g_1	2.990	1.0
g_2	0.419	0.90
α	2.0	2.5
n_0	0.6/cc	0.46/cc
E	500 kev	300 kev

REFERENCES

Akasofu, S. -I., and J. C. Cain, A model storm-time proton belt, Paper presented at the 43rd annual meeting, A.G.U., Washington, April 25-28, 1962a.

Akasofu, S. -I. and J. C. Cain, The magnetic field of the radiation belts, J. Geophys. Research, 67, 4078-4080, 1962b.

Akasofu, S. -I., J. C. Cain, and S. Chapman, The magnetic field of a model radiation belt, numerically calculated, J. Geophys, Research, 66, 4013-4026, 1961.

Akasofu, S. -I., J. C. Cain, and S. Chapman, The magnetic field of the quiet-time proton belt, J. Geophys. Research, 67, 2645-2647, 1962.

Akasofu, S. -I., and S. Chapman, The ring current, geomagnetic disturbance, and the Van Allen radiation belts, J. Geophys. Research, 66, 1321-1350, 1961.

Akasofu, S. -I., W. C. Lin, and J. A. Van Allen, The anomalous entry of low-rigidity solar cosmic rays into the geomagnetic field, J. Geophys. Research, 68, 5327-5338, 1963.

Bame, S. J., J. P. Conner, H. H. Hill, and F. E. Holly, Protons in the outer zone of the radiation belt, J. Geophys, Research, 68, 55-64, 1963.

Beard, D. B., Self-consistent calculation of the ring current, J. Geophys. Research, 67, 3615-3616, 1962.

Cahill, L. J., and P. G. Amazeen, The boundary of the geomagnetic field, J. Geophys. Research, 68, 1835-1843, 1963.

Davis, L. R., R. A. Hoffman, and J. M. Williamson, Observations of protons trapped above 2 earth radii, Paper presented at the 45th annual meeting, A.G.U., Washington, April 21-24, 1964. To be published.

Davis, L. R. and J. M. Williamson, Low-energy trapped protons, Space Research III, Proc. Third Intern. Space Sci. Symp., Washington, 1962, ed. W. Priester, 365-375, North-Holland Pub. Co., Amsterdam, 1963.

Dessler, A. J., W. B. Hanson, and E. N. Parker, Formation of the geomagnetic storm main-phase ring current, J. Geophys. Research, 66, 3631-3638, 1961.

Kellogg, P. J., and J. R. Winckler, Cosmic ray evidence for a ring current, J. Geophys. Research, 66, 3991-4001, 1961.

Liemohn, H., The lifetime of radiation belt protons with energies between 1 kev and 1 mev, J. Geophys. Research, 66, 3593-3595, 1961.

Naugle, J. E., and D. A. Kniffen, Variations of the proton energy spectrum with position in the inner Van Belt., J. Geophys. Research, 68, 4065-4078, 1963.

Parker, E. N., Newtonian development of the hydromagnetic properties of ionized gases of low density, Phys. Rev., 107, 924-933, 1957.

Ray, E. C., Cosmic-ray cut-offs at high latitudes, J. Geophys. Research, 69, 1737-1741, 1964.

Stratton, J. A., Electromagnetic Theory, McGraw-Hill Book Co., New York, 1941.

Vestine, E. H., Low-level geomagnetic ring-current effects, J. Geophys. Research, 68, 4897-4907, 1963.

FIGURE CAPTIONS

Figure 1a. The source of the current due to the second term in equation 7. The eastward current between the two curved lines of force is caused by the crowding together of the circular orbits on the concave sides of the lines.

Figure 1b. The source of the current arising from the last term in equation 7. If the particle intensity about the line of force further away from the earth exceeds that about the closer line, indicated by the relative weights of the gyration circles, a net eastward current results in the region between the two lines of force.

Figure 2. The projection on the earth's equatorial plane of pass number 10 on August 27 and 28, 1961.

Figure 3. The planetary magnetic three-hour-range index K_p for the period during which the data used in this study were acquired.

Figure 4. Double sloped integral proton spectrum employed in the calculation of the momentum integral.

Figure 5. Sample fits of the equatorial pitch angle distributions to the function $\sin \alpha$ for the regions 90° to 30° and 30° to 0°.

Figure 6. The pitch angle parameter α as a function of energy for L values of 2 and 4.

Figure 7. The values of α as a function of L for the two pitch angle ranges derived for the particles having the average momentum on the given L shell.

Figure 8. The omnidirectional momentum flux ψ (L) for each of the two pitch angle ranges in units of gm/cm-sec^2 (or ergs/cm^3).

Figure 9. A contour plot of the total electric current in a magnetic meridian plane derived for protons with energies above 100 kev. The currents, expressed as X^y signify $X \cdot 10^y$. To convert currents from esu/cm^2-sec to amps/km^2, multiply by three.

Figure 10. The contributions of each of the terms in equation 23 to the total current for two different L shells.

Figure 11. A smoothed version of the electric current contour plot to illustrate the dominant features of the electric current distribution.

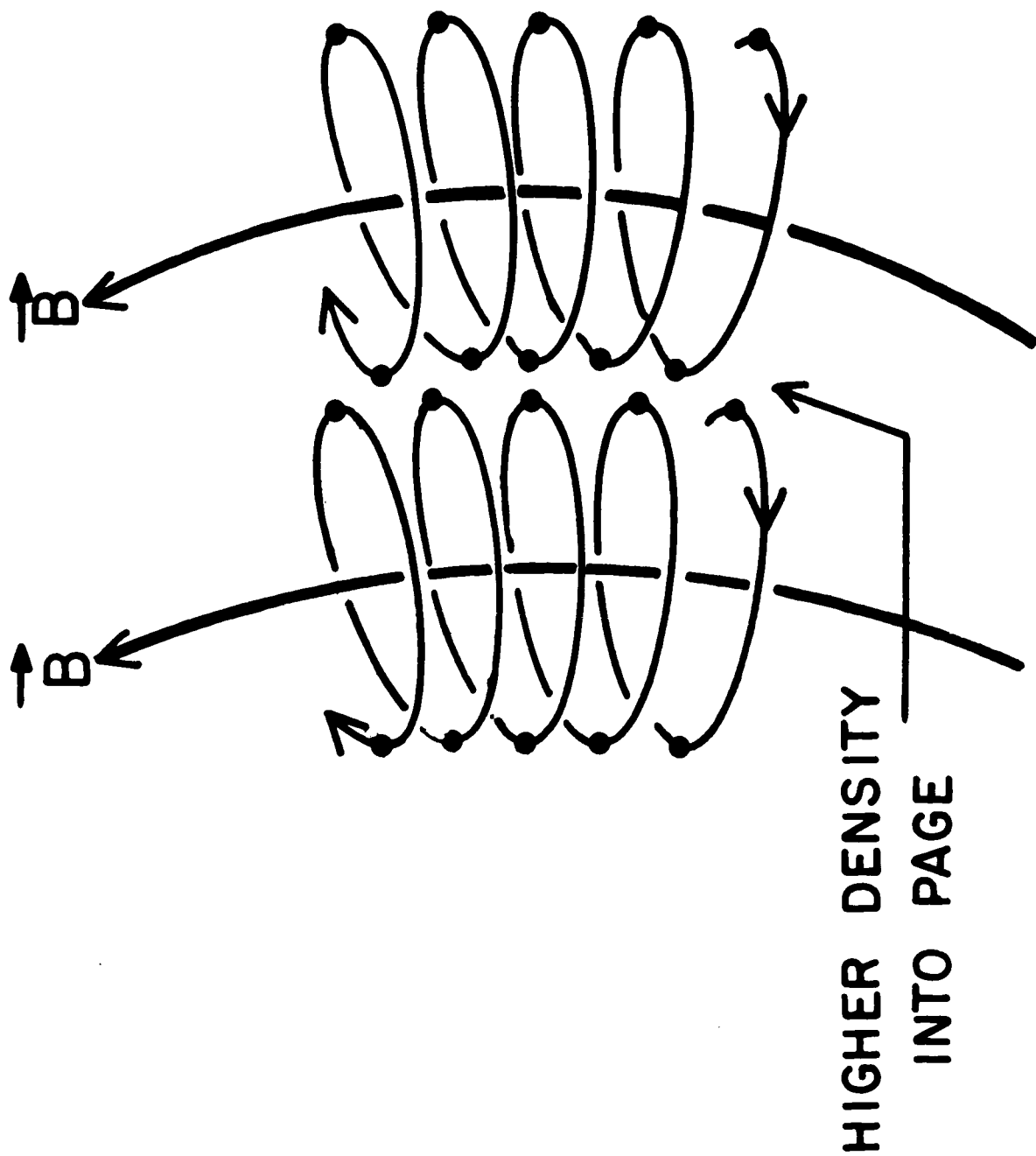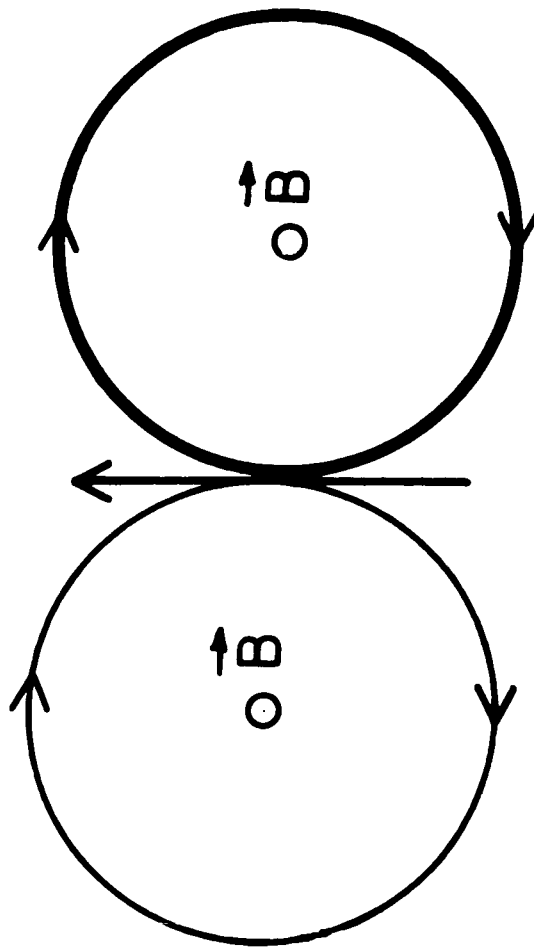Figure 12. Vector magnetic field on a meridian plane due to the proton ring current.

↑B

↑B

HIGHER DENSITY
INTO PAGE

Fig. 1a

NET EASTWARD CURRENT

EARTH NORTH

Fig. 1b

Fig. 2

Fig. 3

N_{OI}

$N(>E)$

e^{-E/E_0}

e^{-E/E_1}

I   100   E'   4500

E (kev)

Fig. 4

Fig. 5

30°-90° EQUATORIAL PITCH ANGLES

⊙ L = 2.5
X L = 4

α

E (kev)

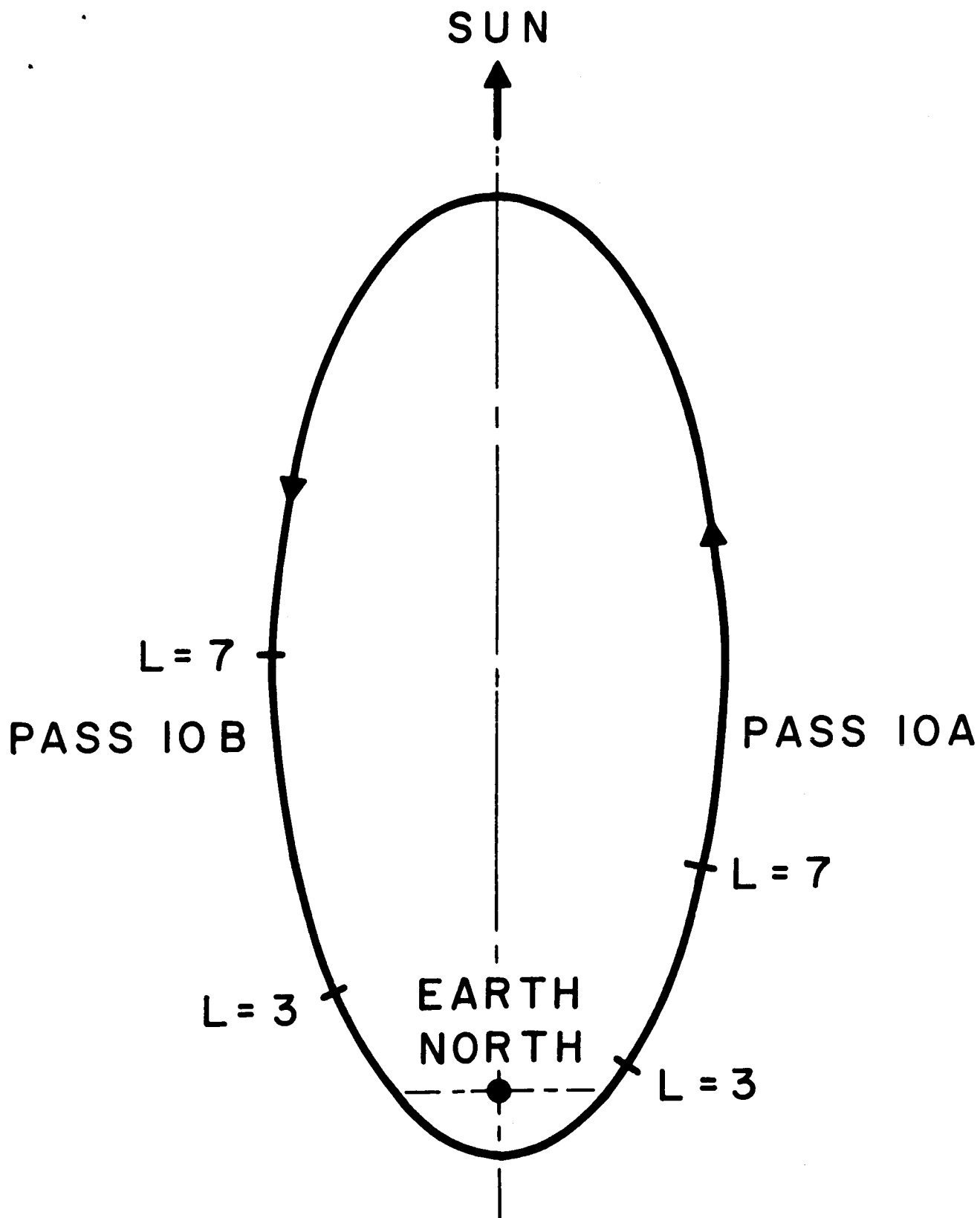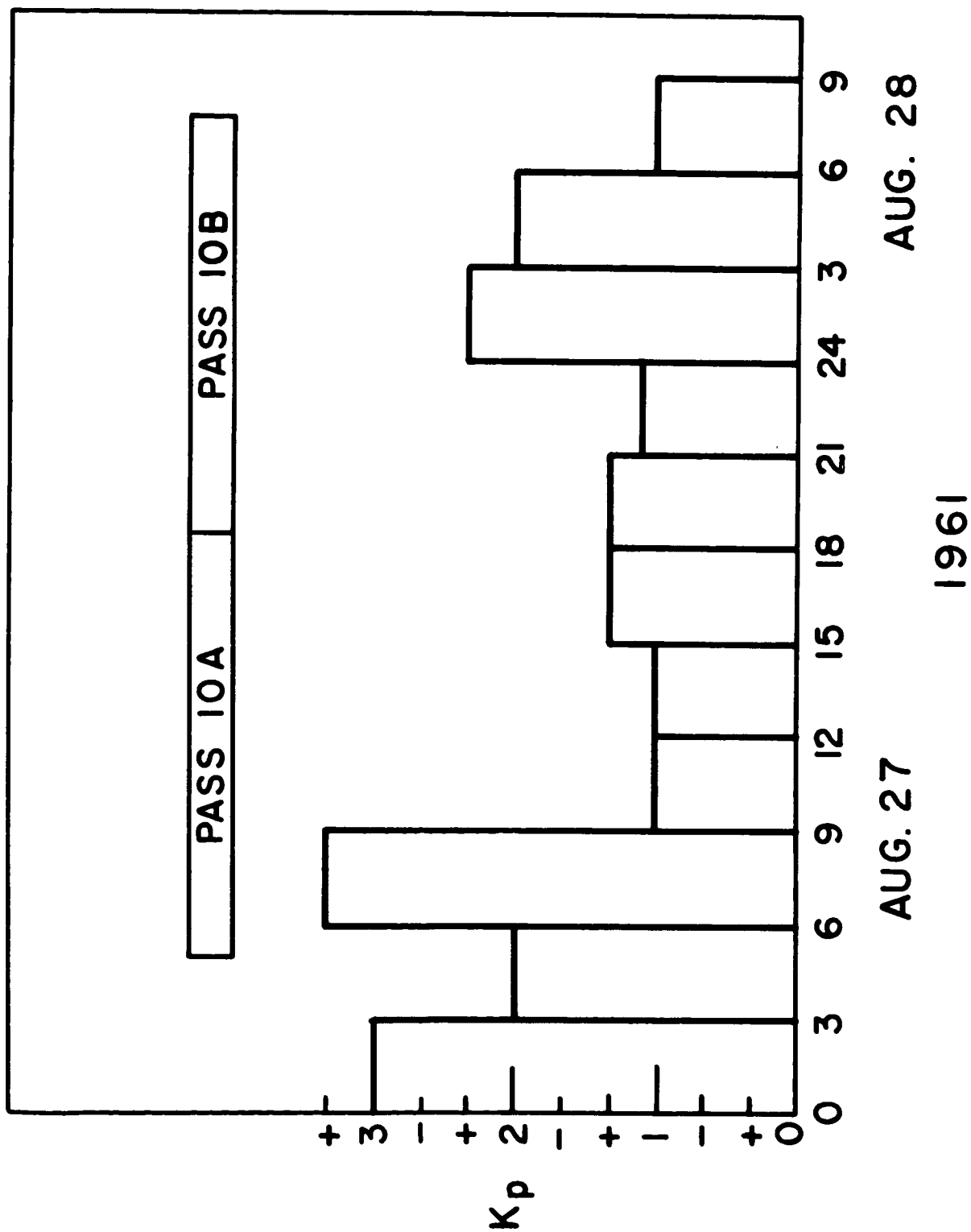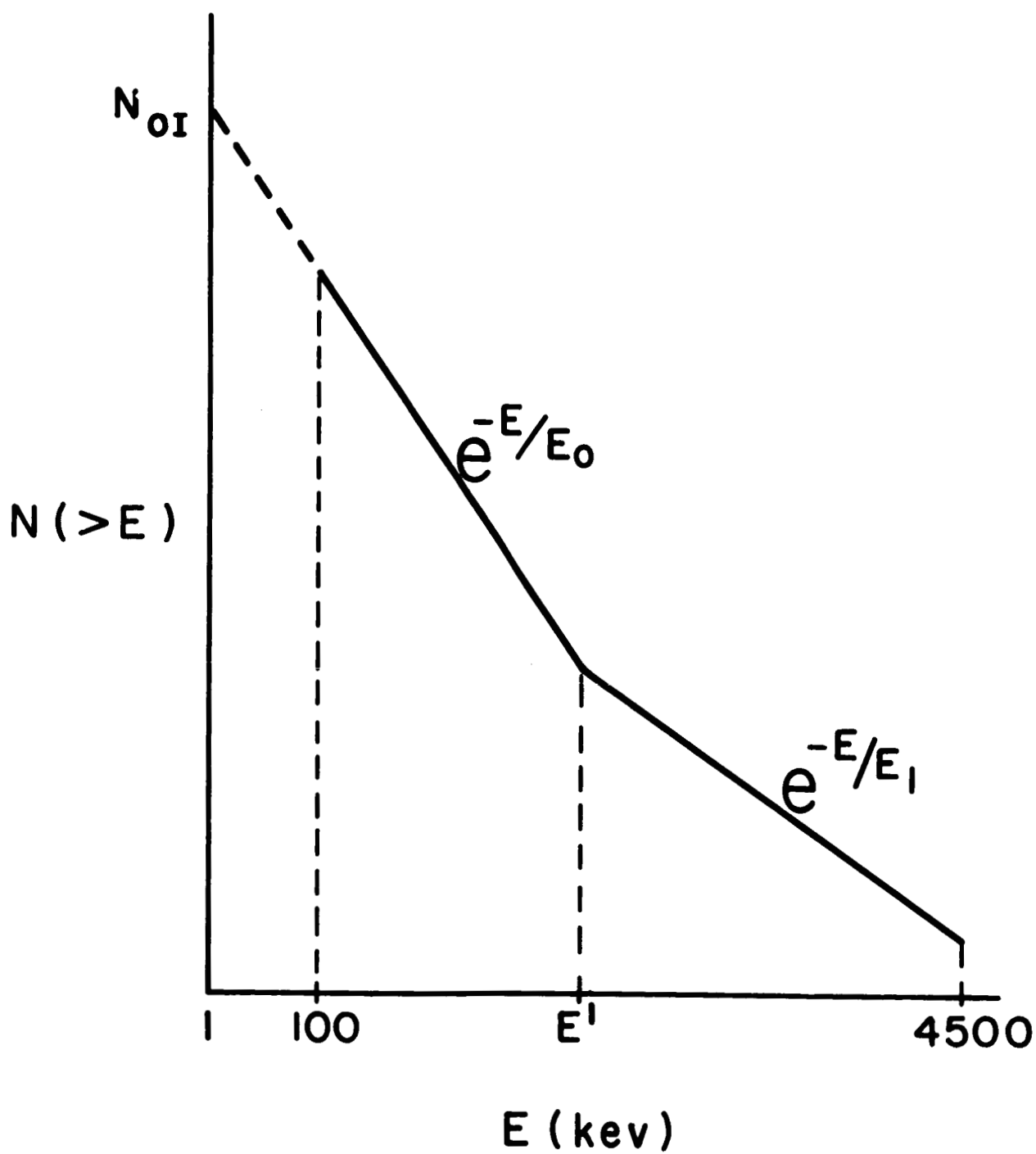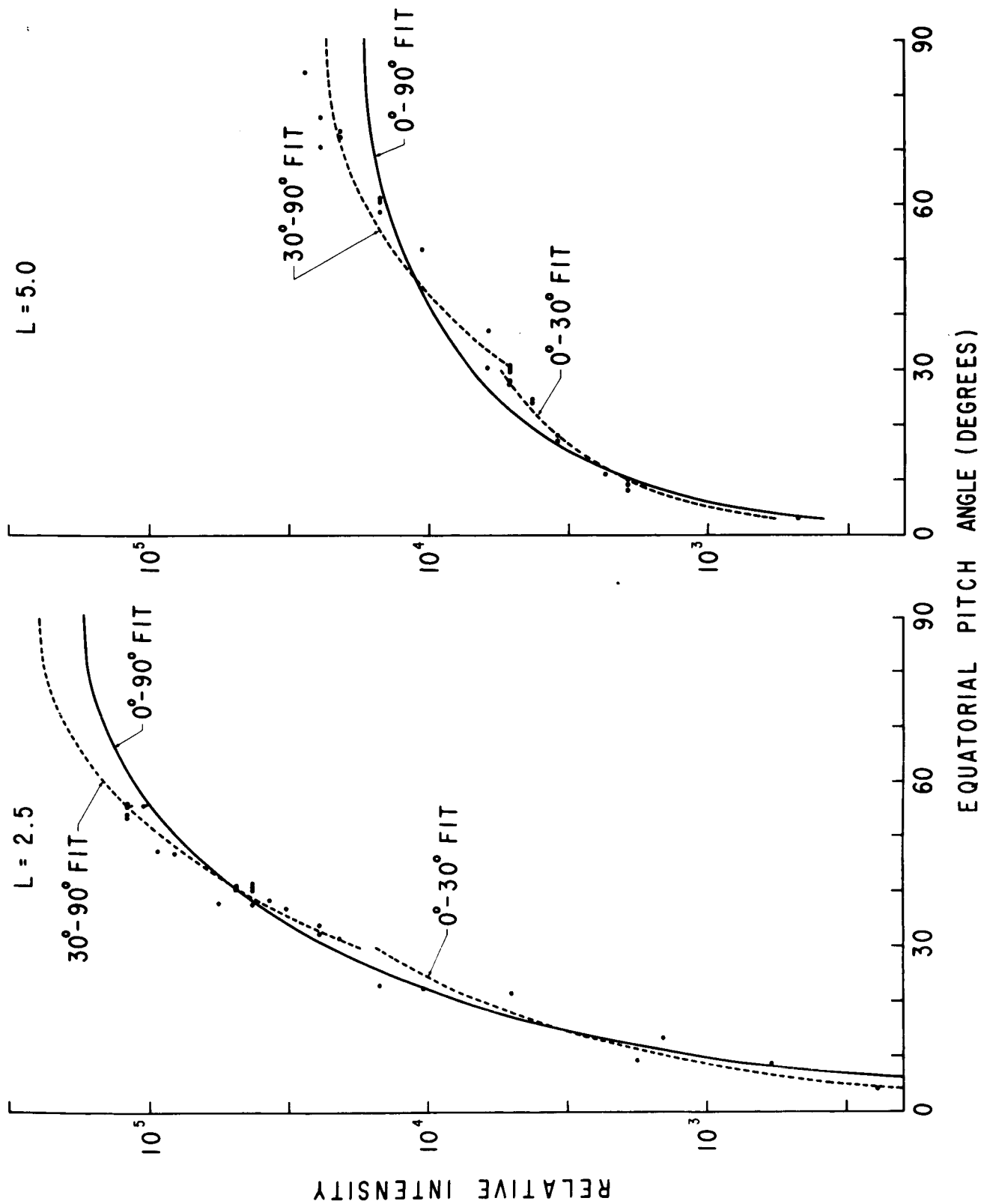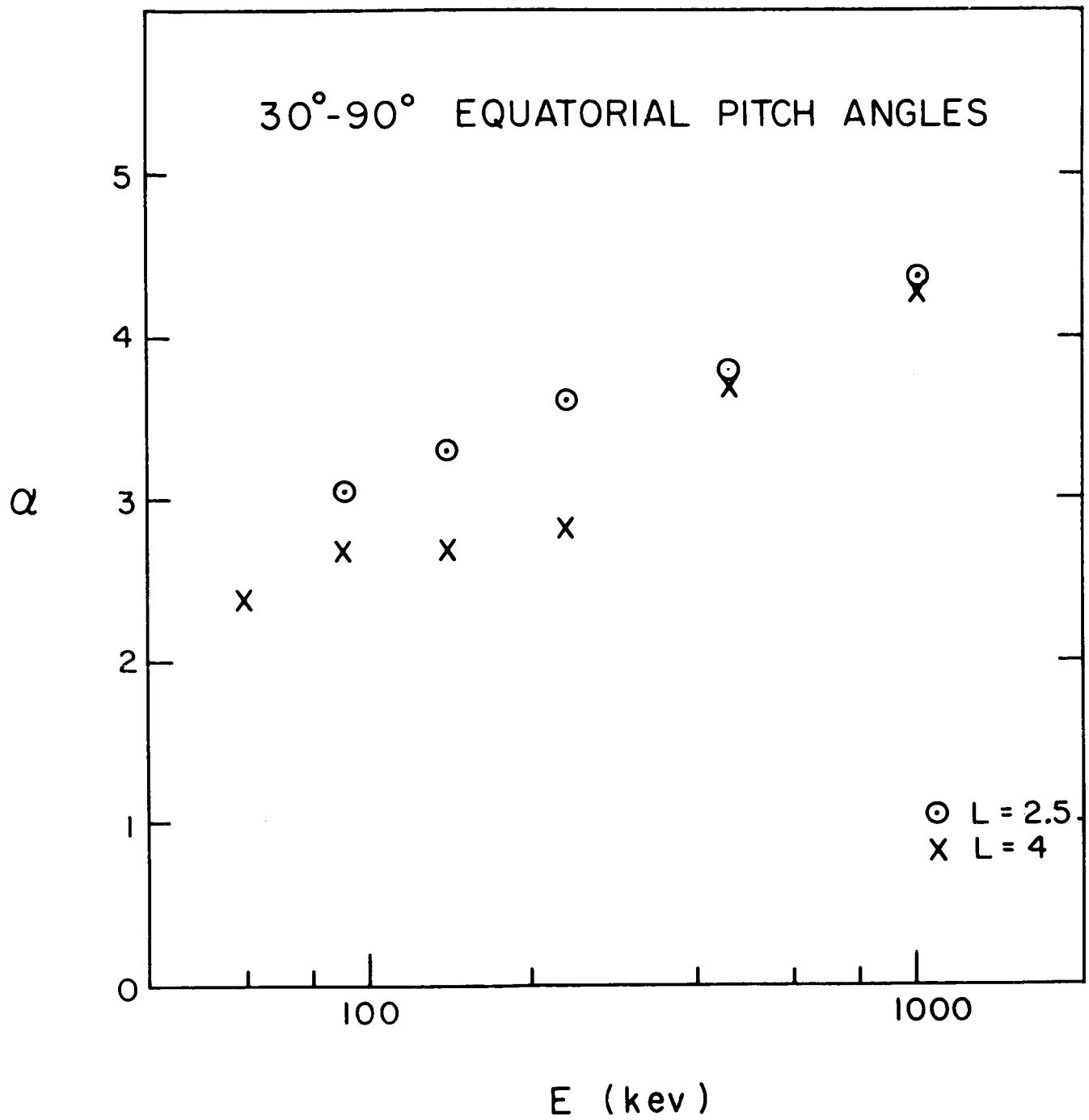Fig. 6

Fig. 7

Fig. 3

Fig. 9

$J_1 \propto L^2 \psi$

$J_2 \propto L^3 \dfrac{d\psi}{dL}$

$J_3 \propto L^3 \psi \dfrac{d\alpha}{dL}$

i- Total current

L = 2.5

EARTH'S SURFACE

L = 5.0

EARTH'S SURFACE

B/B_o

B/B_o

Current in 10^{-4} esu/sec·cm^2

Fig. 10

Fig. 11

EARTH

25 γ

Fig. 12